PHYSICAL CHEMISTRY

Roaming in highly excited states: The central atom elimination of triatomic molecule decomposition

Zhenxing Li[1]†, Yan-lin Fu[1]†, Zijie Luo[1,2], Shuaikang Yang[1], Yucheng Wu[1,3], Hao Wu[1,3], Guorong Wu[1], Weiqing Zhang[1], Bina Fu[1,3,5]*, Kaijun Yuan[1,3,5]*, Donghui Zhang[1,3,5], Xueming Yang[1,4,5]

Chemical reactions are generally assumed to proceed from reactants to products along the minimum energy path (MEP). However, straying from the MEP—roaming—has been recognized as an unconventional reaction mechanism and found to occur in both the ground and first excited states. Its existence in highly excited states is however not yet established. We report a dissociation channel to produce electronically excited fragments, $S(^1D)+O_2(a^1\Delta_g)$, from SO_2 photodissociation in highly excited states. The results revealed two dissociation pathways: One proceeds through the MEP to produce vibrationally colder $O_2(a^1\Delta_g)$ and the other yields vibrationally hotter $O_2(a^1\Delta_g)$ by means of a roaming pathway involving an intramolecular O abstraction during reorientation motion. Such roaming dynamics may well be the rule rather than the exception for molecular photodissociation through highly excited states.

The identification of molecular mechanisms and pathways for chemical reactions is one of the intellectual cornerstones and central goals of chemistry. It has long been assumed that chemical reactions occur along minimum energy paths (MEPs) that are characterized by a transition state (TS) in the form of a well-defined saddle point on the potential energy surface (PES). However, an unusual roaming path has recently come to light, one that strays from MEPs entirely. Instead, a frustrated bond cleavage leaves part of the molecule without sufficient energy to escape and orbits the remaining fragment until encountering a reactive site to form the products through intramolecular abstraction. Roaming reactions, first identified in joint experimental and theoretical studies of formaldehyde photodissociation in 2004 (*1*), have since been recognized as a generic aspect of chemical reactivity (*2*–*7*). Evidence of roaming dynamics has been observed in a broad variety of molecular systems and with different roaming fragments (*8*–*22*). Thus far, in all instances roaming has been observed only in the ground state and the first excited state of the parent molecule, resulting in the formation of ground-state products. No roaming phenomena have been detected in highly excited states nor have they led to the generation of electronically excited products.

Triatomic molecules have served as textbook examples for the study of unimolecular reaction dynamics and recent advances show that we still have much to learn from these typical molecules (*23*). Chemical intuition suggests that the absorption of a high-energy photon by a triatomic molecule such as CO_2 would give rise to a single bond fission and produce CO+O fragments. The central atom elimination process, $C+O_2$, would not happen because CO possesses a much more stable diatomic bond than O_2. However, Lu *et al.* (*24*) reported recently that O_2 production occurred after CO_2 was highly excited. Two possible mechanisms for such photoinduced central atom elimination were considered: One involves dissociation from a transition state accessed by prior structural rearrangements of the molecule and the other invokes fission of one chemical bond followed by an intramolecular reaction between the resulting fragments, i.e., roaming. Another case of central atom elimination in the OClO molecule, which led to $Cl(^2P)+O_2(^1\Delta_g)$, exhibited notable mode-specific dynamics (*25*, *26*). The theoretical analysis, based on potential energy mapping in C_{2v} symmetry, elucidated a direct O atom approach path without providing any evidence of a roaming mechanism (*27*). In addition, recent studies of $C(^3P)$ elimination from CS_2 have been viewed as an example of the transition state mechanism (*28*, *29*) and a roaming mechanism was suspected to account for the almost isotropic recoil velocity distributions observed for the $C(^3P)$ + SO(X) products formed when exciting OCS just above the energetic threshold for this process (*30*). The prediction of these roaming mechanisms was based on static structural and energy analysis but the verification of roaming mechanisms in a central atom elimination channel such as this one has not been achieved experimentally or theoretically from a dynamical perspective, to the best of our knowledge. The challenge involves the high threshold for eliminating the central atom in many triatomic molecules [acquiring high excitation photon energy up to the vacuum ultraviolet (VUV) region] and high density of nonadiabatic couplings between many excited PESs, which prevents distinguishing roaming and transition-state paths to the same products. Thus, it remains unclear to what extent the roaming mechanism contributes to the photodissociation of triatomic molecules.

SO_2, a typical triatomic molecule, is an important species in Earth's atmosphere. The photochemistry of SO_2 has been recognized as the origin of the sulfur mass-independent fractionation (S-MIF) in ancient rock samples (*31*, *32*). SO_2 has two strong absorption bands in the UV region: one is between 185 nm and 235 nm, corresponding to the transition from ground $1^1A'$ to $2^1A'$ states ($2^1A'\leftarrow1^1A'$) (*33*); the other is between 240 to 350 nm as a result of the transition to the $2^1A''$ state, which couples with the $1^1A''$ state through a conical intersection ($1^1A''/2^1A''\leftarrow1^1A'$) (*34*, *35*). At shorter wavelengths, the diffuse absorption bands are assigned to transitions to high Rydberg states (*36*). Below 219 nm, SO_2 has been assumed to predissociate exclusively to SO and O fragments, through nonadiabatic couplings between low-lying repulsive triplet and singlet states (*37*, *38*). The central atom elimination yielding $S+O_2$ is energetically possible but has not been observed until recently. Rösch *et al.* (*39*, *40*) provided the first evidence for the $S(^3P) + O_2$ channel from SO_2 photolysis at 193 nm, and Chang *et al.* (*41*) displayed the experimental observation of the $S(^1D)+O_2$ channel in the wavelength range of 120 to 160 nm. Both processes could be of great importance for understanding the origin of O_2 in Earth's prebiotic primitive atmosphere. However, questions regarding the prevalence of roaming reactions in highly excited states of molecules persist in these previous studies.

We performed detailed experiments on SO_2 photodissociation around 133 nm. The experimental results revealed previously undetected bimodal $O_2(a^1\Delta_g)$ vibrational distributions. Insights from classical trajectory calculations on a highly excited state PES demonstrated two distinctive dissociation pathways: One proceeds through the MEP to produce vibrationally colder $O_2(a^1\Delta_g)$; the other strays from the MEP, roams around varied configuration spaces of flat potential energy regions, and abstracts another O atom to form the highly vibrationally excited $O_2(a^1\Delta_g)$. The latter contributed nearly one half of the total yield of $O_2(a^1\Delta_g)$ products. The results represent a clear example of roaming in highly excited states of a triatomic molecule, which we expect to be general.

Experimental evidence of roaming pathway in highly excited states

The experiments were carried out using the time-sliced velocity mapped ion (TS-VMI) imaging method combined with the intense, pulsed

[1]State Key Laboratory of Molecular Reaction Dynamics and Dalian Coherent Light Source, Dalian Institute of Chemical Physics, Chinese Academy of Sciences, 457 Zhongshan Road, Dalian 116023, P. R. China. [2]Marine Engineering College, Dalian Maritime University, Liaoning 116026, P. R. China. [3]University of Chinese Academy of Sciences, Beijing 100049, P. R. China. [4]Department of Chemistry and Center for Advanced Light Source Research, College of Science, Southern University of Science and Technology, Shenzhen 518055, P. R. China. [5]Hefei National Laboratory, Hefei 230088, P. R. China.
*Corresponding author. Email: bina@dicp.ac.cn (B.F.); kjyuan@dicp.ac.cn (K.Y.)
†These authors contributed equally to this work.

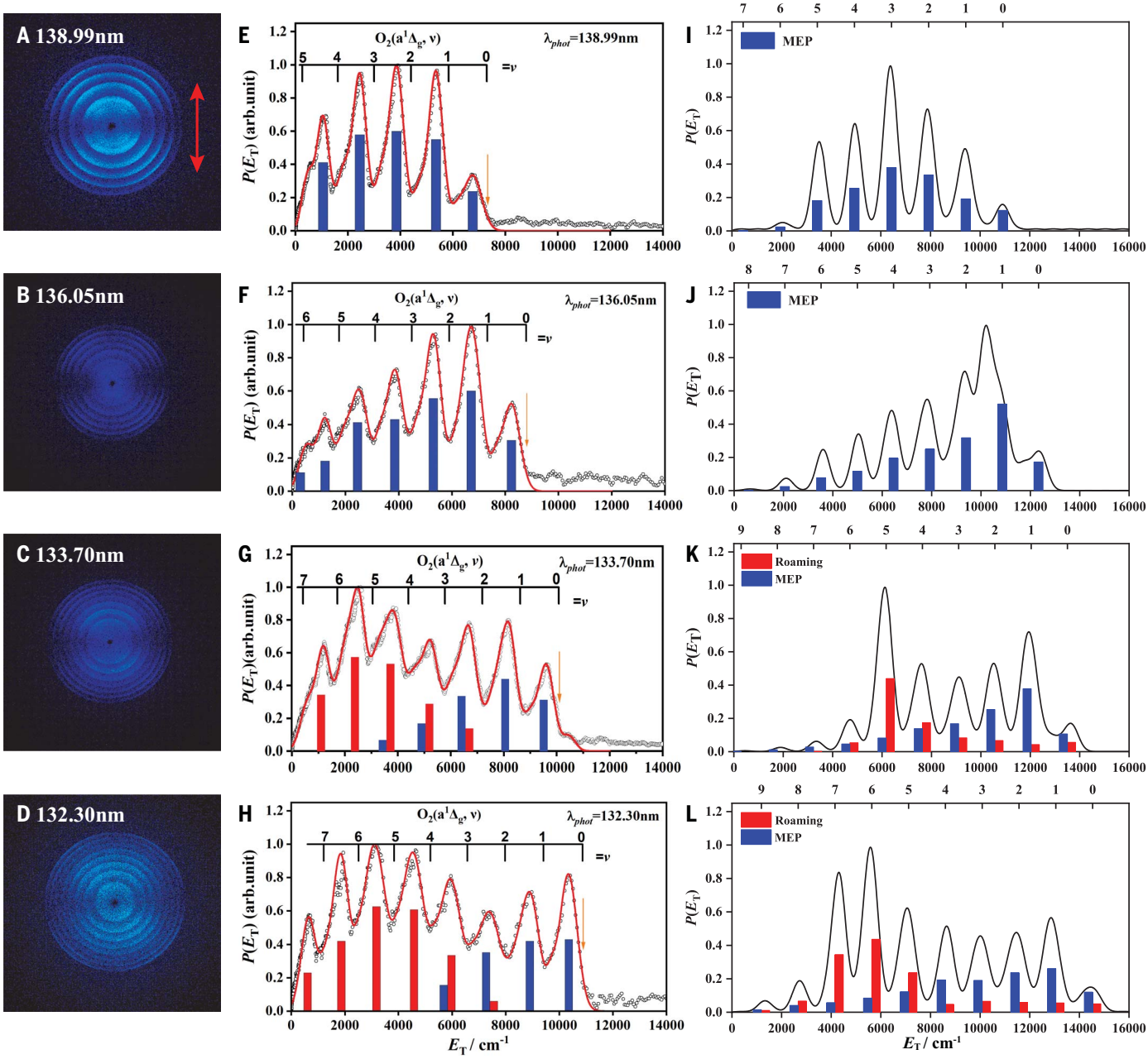

Fig. 1. Experimental and theoretical data for translational energy distributions of S(^{1}D) + O_2($a^1\Delta_g$) from SO_2 photodissociation. The left column shows the time-sliced velocity mapped ion images with photolysis wavelengths of (**A**) 138.99 nm, (**B**) 136.05 nm, (**C**) 133.70 nm, (**D**) 132.30 nm. The red double arrow indicates the polarization direction of the photodissociation laser, ε. The center column (**E** to **H**) displays the product total translational energy distribution [$P(E_T)$] spectra derived from those images, along with the best-fit simulation of the spectra, in red. The superposed combs indicate the E_T values associated with formation of the various O_2($a^1\Delta_g$, v). The stick spectra in blue and red shown underneath the experimental curves are two distinct vibrational state distributions of O_2 returned by fitting. The right column (**I** to **L**) indicates the $P(E_T)$ spectra returned by theoretical calculations and the corresponding vibrational state distributions. Both experimental and theoretical results show a bimodal vibrational distribution of O_2 ($a^1\Delta_g$) products at 133.70 and 132.30 nm. MEP, minimum energy path.

VUV free electron laser (FEL), at the Dalian Coherent Light Source (DCLS) (*41*, *42*). SO_2 in a molecular beam of Ar was briefly excited to a Rydberg state by the output of the VUV FEL. The S atom fragments in the electronically excited ^{1}D state were then resonantly ionized at λ = 130.092 nm, which was generated by a tabletop VUV source from a difference frequency four-wave mixing (FWM) scheme, involving two 212.556-nm photons and one 580.654-nm photon that overlapped in a Kr gas cell. An off-axis biconvex LiF lens, serving as the exit window of the FWM cell, was used to deflect the 212.556-nm and 580.654-nm laser beams, ensuring that only the VUV FEL and the 130.092-nm beam passed through the photodissociation/photoionization region. Thus, other S atom elimination processes, such as the secondary dissociation from SO primary fragments or the three-body dissociation, could be excluded. Post ionization, the S(^{1}D) products were detected by the VMI detector.

Figure 1 shows typical raw images of the S(^{1}D) photofragment recorded following photolysis

of SO_2 at VUV wavelengths of 138.99 nm, 136.05 nm, 133.70 nm, and 132.30 nm (Fig. 1, A, B, C, and D, respectively). An additional eight images in the wavelength range of 132 to 138 nm are displayed in figs. S1 and S2 in the supplementary materials (SM). The red double arrow in Fig. 1A is the polarization direction of the VUV photolysis laser. All observed images were pump probe- and molecular beam–dependent. Well-resolved, concentric rings with different intensities were clearly observable in the displayed images. These structures could be readily assigned to populations of different rovibrational states of the coproduct O_2. The images also displayed orbital alignment of $S(^1D)$ products (*43*). The effect of orbital polarization will be discussed in future studies. Our focus in the present study is solely on the product velocity distribution in the SO_2 photodissociation.

The VMI images obtained in the experiment were used to determine the velocity distribution of the $S(^1D)$ products. These distributions were then converted to total product translational energy distributions [$P(E_T)$] of the S (^1D) + O_2 channel using the law of linear momentum conservation. Figure 1, E to H displays the $P(E_T)$ distributions obtained by integrating signals over all angles in the respective images. The internal energy distributions of the O_2 coproduct could then be obtained from the corresponding $P(E_T)$ distributions using the law of energy conservation.

The thermochemical threshold for the $S(^1D)$ + $O_2(a^1\Delta_g)$ product channel is ~8.06 eV (corresponding to excitation wavelength of λ ~153.76 nm) (*44*). The maximum translational energy (E_T values) associated with the formation of O_2 ($a^1\Delta_g$, v = 0, j = 0) is marked by orange arrows (Fig. 1, E to H). The onset of the strong progressions in the $P(E_T)$ distributions clearly matches the threshold of the $S(^1D)$ + $O_2(a^1\Delta_g)$ product channel, providing unambiguous evidence for the formation of the electronically excited molecular oxygen in the VUV photodissociation of SO_2. Based on the vibrational term values calculated from the spectroscopic constants (*44*), the energy combs representing each vibrational level of $O_2(a^1\Delta_g)$ products were labeled in Fig. 1, E to H. It is worth noting that there were small signals in the high translational energy beyond the onset of the $O_2(a^1\Delta_g, v = 0)$, which could be attributed to the $S(^1D)$ + $O_2(X^3\Sigma_g^-)$ channel as the ground electronic state, $O_2(X^3\Sigma_g^-)$, is 7882 cm^{-1} lower than the first electronically excited state, O_2 ($a^1\Delta_g$) (*44*). The vibrational progressions for the $O_2(X^3\Sigma_g^-)$ products extended to the low translational energy region but its relative populations were quite small.

The best fitting of the $P(E_T)$ distributions yielded the vibrational state population distributions of the $O_2(a^1\Delta_g)$ products, which are displayed in the stick spectra underneath the experimental curves (Fig. 1, E to H). At 138.99 nm and 136.05 nm, the $O_2(a^1\Delta_g)$ fragments had somewhat colder vibrational state distributions, with the peak at v = 1~2, similar to that observed in previous studies at longer photolysis wavelengths (*41*). By contrast, at 133.70 nm and 132.30 nm an unexpected bimodal vibrational energy distribution for the $O_2(a^1\Delta_g)$ products was clearly observed, peaking at v = 0~1 and v = ~5. Figures S1 and S2 further demonstrate that such bimodal vibrational state population distribution could only be observed at around 132 to 134 nm photolysis. The fraction of high vibrational excited $O_2(a^1\Delta_g)$ products was determined to be ~0.4 to 0.6. To the best of our knowledge, no distinguishable bimodal vibrational distribution has been observed previously in SO_2 photodissociation at shorter photolysis wavelengths (*41*), or in other triatomic molecular photodissociation processes (*23*–*27*). The similarity between the energy distribution within the products of $S(^1D)$ + $O_2(a^1\Delta_g)$ channel in the range of 132 to 134 nm and the molecular products resulting from formaldehyde photolysis (*1*) leads to speculation that the high vibrational excited $O_2(a^1\Delta_g)$ was likely produced through the roaming dynamics.

Theoretical illustration of roaming dynamics in highly excited states

To characterize the detailed dissociation mechanism of VUV SO_2 photolysis from highly excited states, we carried out extensive MRCI-F12+Q/AVTZ calculations and developed the full-dimensional PESs of multiple electronic states by fundamental invariant-neural network (FI-NN) fitting (*45*). The vertical excitation energies of the singlet and triplet states in A″ symmetry and A′ symmetry, respectively, as well as the related dissociation paths to SO+O and S+O_2 channels, have been drawn in fig. S3. The density of electronic states of SO_2 from 8 eV to 10 eV near the Franck-Condon region was very high, which made it easy to transfer between adjacent states through internal conversions and/or intersystem crossings. Two different processes could be identified based on the full-dimensional optimization on the 12 global PESs in A″ symmetry and 12 PESs in A′ symmetry (figs. S4 and S5): One process proceeds through the direct approaching of the two O atoms and finally the ejection of O_2, and the other proceeds by means of the initial leaving of one O atom and further abstraction of another O atom. These two different processes, through S-O-O or *cyclic*-SO_2 intermediates, were seen from many paths with transitions by internal conversions or intersystem crossings of electronic states, leading to the $S(^1D)$ + O_2 ($a^1\Delta_g$) channel, which supports the experimental observations from VUV SO_2 photodissociation.

Figure 2 depicts one dissociation route with the lowest number of nonadiabatic transitions through the singlet-state manifold, in which SO_2 is photo-excited to the $5^1A''$ state, and then proceeds through nonadiabatic transition to the $3^1A''$ state, where it finally dissociates adiabatically to form the $S(^1D)$ + $O_2(a^1\Delta_g)$ channel. A minimum-energy conical intersection (MECI) between $5^1A''$ and $3^1A''$, which is also intersected by $4^1A''$, was identified by geometry optimizations using the Lagrange-Newton method (*47*), as shown in fig. S6. The dissociation on the $3^1A''$ state could proceed through the S-O-O or cyclic-SO_2 intermediates based on the potential energy mapping. The intrinsic mechanisms associated with the bimodal product distribution could then be revealed by accurate dynamics simulations on the full-dimensional PES.

Quasi-classical trajectories were carried out, initiating from the MECI with microcanonical samplings of velocities relevant to the experimental photoexcitation energy around 133 nm (*47*), which further evolved on the adiabatic PES of the $3^1A''$

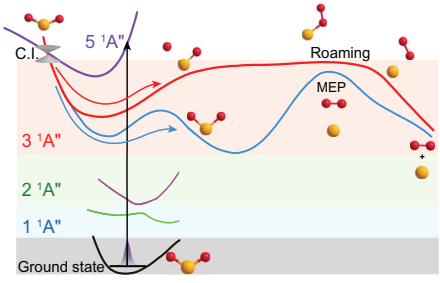

Fig. 2. One dissociation route leading to $S(^1D)$ + $O_2(a^1\Delta_g)$ with least nonadiabatic transitions by means of the singlet-state manifold at 132.30 nm. The schematic of potential energy curves for the ground and four excited states in A″ symmetry are connected with the MEP and roaming paths on the $3^1A''$ state. The MECI between $5^1A''$ and $3^1A''$ states is indicated by a circular cone.

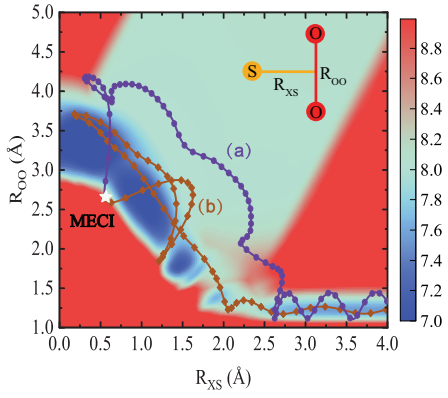

Fig. 3. Projections of typical trajectories on a contour plot of PES. Projections of trajectories representing the roaming dynamics (**A**) and MEP (**B**) on the contour plot of $3^1A''$ PES, exhibited as functions of the distance between midpoint of O-O (X) and S (R_{XS}), and the O-O distance (R_{OO}). The contours are calculated with the other degrees of freedom fully optimized.

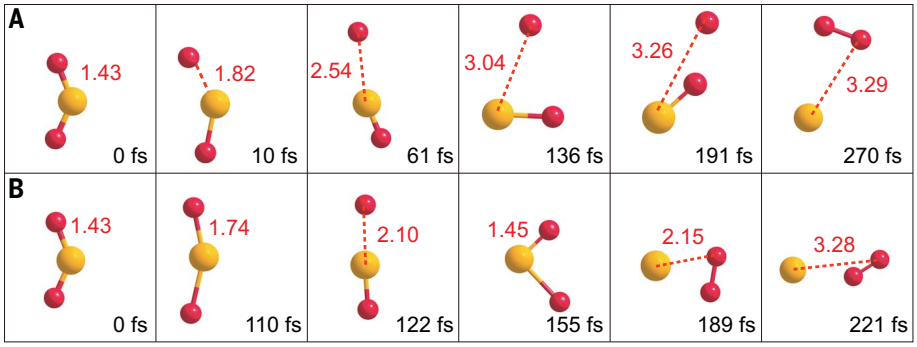

Fig. 4. Snapshots of two sample trajectories. Snapshots of the roaming trajectory (**A**) (upper panel) and nonroaming trajectory (**B**) (bottom panel) at the time indicated (fs). The S-O distance is also indicated.

state to produce the $S(^1D) + O_2(a^1\Delta_g)$ channel. The main feature of bimodal characters in both the product kinetic energy distribution and vibrational state distribution has been reproduced by trajectory calculations with the final conditions analyzed in a quantum spirit on the $3^1A''$ state (Fig. 1, I to L). By contrast, there was no bimodal distribution of $O_2(a^1\Delta_g)$ products from photodissociation at 136 and 139 nm, in good accord with experimental results. It is worth noting that the dissociation limit of $S(^1D) + O_2(a^1\Delta_g)$ product channel on the global PES based on the MRCI-F12+Q/AVTZ level of theory is ~0.4 eV lower than the experimental results, indicating more available energy from theory depositing to the $S(^1D) + O_2(a^1\Delta_g)$ product channel.

The trajectories revealed a mechanism for the $S(^1D) + O_2(a^1\Delta_g)$ channel as an alternative to the traditional MEP. This O-atom roaming mechanism strays away from the MEP and is initiated by the frustrated dissociation to form SO+O; the O atom then wanders around varied configuration spaces of the flat potential energy regions and ultimately abstracts another O atom to form the $O_2(a^1\Delta_g)$ product. Projections of one typical roaming trajectory and one nonroaming trajectory onto the contour plot of PES are depicted in Fig. 3 and the corresponding snapshots of two sample trajectories are illustrated in Fig. 4. One trajectory shows that the dissociation proceeded through the O atom meandering near the SO+O product region first and then turned back to produce high-vibrational excited $O_2(a^1\Delta_g)$. The other, by contrast, shows that the dissociation effectively followed the MEP to form $O_2(a^1\Delta_g)$ with low-vibrational excitation. It was found that the O atom could be pulled out, up to a distance of 3.26 Å, from the S atom in this roaming trajectory. The two considerably different mechanisms were clearly responsible for the bimodal distribution observed in the experimental results. In addition, the roaming pathway accounted for nearly one half of the total yield of $O_2(a^1\Delta_g)$ at around 133 nm, similar to experimental observations and demonstrating the substantial competing role and fundamental importance of the roaming mechanism in VUV photodissociation of SO_2. The animations of two sample trajectories are given in movies S1 and S2. The energies along the contour plot of PES as well as the two representative trajectories could be well-reproduced by MRCI-F12 calculations (figs. S7 and S8), indicating the accuracy of the PES and the dynamical results.

Conclusions

In summary, we presented the first direct dynamical evidence of roaming for photodissociation of a triatomic molecule originating from a highly excited electronic state, which leads to the formation of an electronically excited S atom and O_2 molecule as observed experimentally and confirmed theoretically. Because roaming yields products through reorientational motion in the long-range region of the potential, the flat potential region that leads to a "self-abstraction" of the incipient radicals to give molecular products is essential. Molecular dissociation in highly excited states involves high-density excited electronic states and complicated nonadiabatic transitions, which very likely contribute to a relatively flat potential energy landscape at long ranges along with coupling to quasi-bound states. Thus, an increased probability of encountering frustrated bond cleavage will promote the likelihood of roaming reactions in highly excited states. This study opens the door for roaming from a highly excited electronic state to produce electronically excited products, which react very differently in the atmosphere, space, and in combustion. As for SO_2, its molecular oxygen production channel has been suggested to contribute to increasing oxygen levels in Earth's early atmosphere. Thus, the roaming mechanism of O_2 production should be incorporated into photochemical models for planets with rich volcanically outgassed SO_2.

REFERENCES AND NOTES

1. D. Townsend *et al.*, *Science* **306**, 1158–1161 (2004).
2. A. G. Suits, *Acc. Chem. Res.* **41**, 873–881 (2008).
3. J. M. Bowman, B. C. Shepler, *Annu. Rev. Phys. Chem.* **62**, 531–553 (2011).
4. N. Herath, A. G. Suits, *J. Phys. Chem. Lett.* **2**, 642–647 (2011).
5. J. M. Bowman, A. G. Suits, *Phys. Today* **64**, 33–37 (2011).
6. J. M. Bowman, *Mol. Phys.* **112**, 2516–2528 (2014).
7. A. G. Suits, *Annu. Rev. Phys. Chem.* **71**, 77–100 (2020).
8. P. L. Houston, S. H. Kable, *Proc. Natl. Acad. Sci. U.S.A.* **103**, 16079–16082 (2006).
9. B. R. Heazlewood *et al.*, *Proc. Natl. Acad. Sci. U.S.A.* **105**, 12719–12724 (2008).
10. M. S. Quinn *et al.*, *Science* **369**, 1592–1596 (2020).
11. C. D. Foley, C. Xie, H. Guo, A. G. Suits, *Science* **374**, 1122–1127 (2021).
12. T. Endo *et al.*, *Science* **370**, 1072–1077 (2020).
13. M. L. Hause, N. Herath, R. Zhu, M. C. Lin, A. G. Suits, *Nat. Chem.* **3**, 932–937 (2011).
14. M. P. Grubb, M. L. Warter, A. G. Suits, S. W. North, *J. Phys. Chem. Lett.* **1**, 2455–2458 (2010).
15. M. P. Grubb *et al.*, *Science* **335**, 1075–1078 (2012).
16. B. Joalland, Y. Shi, A. Kamasah, A. G. Suits, A. M. Mebel, *Nat. Commun.* **5**, 4064 (2014).
17. B. Fu, J. M. Bowman, H. Xiao, S. Maeda, K. Morokuma, *J. Chem. Theory Comput.* **9**, 893–900 (2013).
18. Y. L. Fu *et al.*, *Chem. Sci.* **11**, 2148–2154 (2020).
19. S. Maeda, T. Taketsugu, K. Morokuma, *J. Phys. Chem. Lett.* **3**, 1900–1907 (2012).
20. A. Matsugi, *J. Phys. Chem. Lett.* **4**, 4237–4240 (2013).
21. A. Li, J. Li, H. Guo, *J. Phys. Chem. A* **117**, 5052–5060 (2013).
22. K. L. K. Lee *et al.*, *Chem. Sci.* **5**, 4633–4638 (2014).
23. Y. Chang, M. N. R. Ashfold, K. Yuan, X. Yang, *Natl. Sci. Rev.* **10**, nwad158 (2023).
24. Z. Lu, Y. C. Chang, Q. Z. Yin, C. Y. Ng, W. M. Jackson, *Science* **346**, 61–64 (2014).
25. E. Bishenden, D. J. Donaldson, *J. Chem. Phys.* **99**, 3129–3132 (1993).
26. H. F. Davis, Y. T. Lee, *J. Chem. Phys.* **105**, 8142–8163 (1996).
27. K. A. Peterson, H.-J. Werner, *J. Chem. Phys.* **105**, 9823–9832 (1996).
28. Z. Li *et al.*, *J. Phys. Chem. Lett.* **12**, 844–849 (2021).
29. T. Trabelsi, M. M. Al-Mogren, M. Hochlaf, J. S. Francisco, *J. Chem. Phys.* **149**, 064304 (2018).
30. W. Chen *et al.*, *J. Phys. Chem. Lett.* **10**, 4783–4787 (2019).
31. S. O. Danielache, C. Eskebjerg, M. S. Johnson, Y. Ueno, N. Yoshida, *J. Geophys. Res.* **113**, D17314 (2008).
32. S. Ono, *Annu. Rev. Earth Planet. Sci.* **45**, 301–329 (2017).
33. C. Lévêque, A. Komainda, R. Taïeb, H. Köppel, *J. Chem. Phys.* **138**, 044320 (2013).
34. A. R. Hoy, J. C. D. Brand, *Mol. Phys.* **36**, 1409–1420 (1978).
35. J. Heicklen, N. Kelly, K. Partymiller, *Rev. Chem. Intermed.* **3**, 315–404 (1980).
36. L. Vušković, S. Trajmar, *J. Chem. Phys.* **77**, 5436–5440 (1982).
37. P. C. Ray, M. F. Arendt, L. J. Butler, *J. Chem. Phys.* **109**, 5221–5230 (1998).
38. A. Okazaki, T. Ebata, N. Mikami, *J. Chem. Phys.* **107**, 8752–8758 (1997).
39. D. Rösch, R. Almeida, B. Sztáray, D. L. Osborn, *J. Phys. Chem. A* **126**, 1761–1774 (2022).
40. D. Rösch, Y. Xu, H. Guo, X. Hu, D. L. Osborn, *J. Phys. Chem. Lett.* **14**, 3084–3091 (2023).
41. Y. Chang *et al.*, *Chem. Sci.* **14**, 8255–8261 (2023).
42. J. Zhou *et al.*, *Nat. Commun.* **11**, 1547 (2020).
43. T. P. Rakitzis, P. C. Samartzis, T. N. Kitsopoulos, *Phys. Rev. Lett.* **87**, 123001 (2001).
44. National Institute of Standards & Technology (NIST), US Department of Commerce, NIST Chemistry WebBook, SRD 69; (2023); http://webbook.nist.gov.
45. R. Chen, K. Shao, B. Fu, D. H. Zhang, *J. Chem. Phys.* **152**, 204307 (2020).
46. N. Koga, K. Morokuma, *Chem. Phys. Lett.* **119**, 371–374 (1985).
47. B. Fu, E. Kamarchik, J. M. Bowman, *J. Chem. Phys.* **133**, 164306 (2010).
48. Z. X. Li *et al.*, Roaming in Highly Excited States: The Central Atom Elimination of Triatomic Molecule Decomposition, Mendeley Data, V1 (2024).

ACKNOWLEDGMENTS

The authors thank the FEL staff for technique support. **Funding:** The experimental work was supported by the National Natural Science Foundation of China (grants 22241304 and 22225303); the National Natural Science Foundation of China (NSFC Center for Chemical Dynamics) (grant 22288201); the Scientific Instrument Developing Project of the Chinese Academy of Sciences (grant GJJSTD20220001), the Innovation Program for Quantum Science and Technology (2021ZD0303304). The theoretical work was supported by the National Natural Science Foundation of China

(grants 22173099 and 22203092), the Innovation Program for Quantum Science and Technology (grant 2021ZD0303305), and the Dalian Innovation Support Program (grant 2021RD05). X.Y. also acknowledges support from the Guangdong Science and Technology Program (grants 2019ZT08L455 and 2019JC01X091) and the Shenzhen Science and Technology Program (grant ZDSYS20200421111001787). **Author contributions:** K.J.Y. and X.M.Y. designed the experiments. Z.X.L., Z.J.L., S.K.Y., and Y.C.W. performed the experiments. W.Q.Z., G.R.W., K.J.Y., and X.M.Y. discussed the experimental results. Y.L.F., H.W., B.N.F., and D.H.Z. performed the theoretical calculations. B.N.F. and K.J.Y. prepared the manuscript. **Competing interests:** The authors declare no competing interests. **Data and materials availability:** All data needed to evaluate the conclusions in this paper are present in the paper or the supplementary materials. All data presented in this paper are deposited at Mendeley Data (*48*).

SUPPLEMENTARY MATERIALS

science.org/doi/10.1126/science.adn3357
Materials and Methods
Figs. S1 to S8
Tables S1 and S2
References (*49*–*60*)
Movies S1 and S2

Submitted 5 December 2023; accepted 18 January 2024
10.1126/science.adn3357